Near-infrared gallium nitride two-dimensional photonic crystal platform on silicon

I. Roland, Y. Zeng, Z. Han, X. Checoury, C. Blin, M. El Kurdi, A. Ghrib, S. Sauvage, B. Gayral, C. Brimont, T. Guillet, F. Semond, and P. Boucaud

Citation: Applied Physics Letters **105**, 011104 (2014); doi: 10.1063/1.4887065
View online: http://dx.doi.org/10.1063/1.4887065
View Table of Contents: http://scitation.aip.org/content/aip/journal/apl/105/1?ver=pdfcov
Published by the AIP Publishing

Near-infrared gallium nitride two-dimensional photonic crystal platform on silicon

I. Roland,[1] Y. Zeng,[1] Z. Han,[1] X. Checoury,[1] C. Blin,[1] M. El Kurdi,[1] A. Ghrib,[1] S. Sauvage,[1] B. Gayral,[2,3] C. Brimont,[4] T. Guillet,[4] F. Semond,[5] and P. Boucaud[1,a)]
[1]*Institut d'Electronique Fondamentale, CNRS - Univ. Paris Sud 11, Bâtiment 220, F-91405 Orsay, France*
[2]*Univ. Grenoble Alpes, INAC-SP2M, CEA-CNRS group "Nanophysique et Semiconducteurs," F-38000 Grenoble, France*
[3]*CEA, INAC-SP2M, CEA-CNRS group "Nanophysique et Semiconducteurs," F-38000 Grenoble, France*
[4]*Université Montpellier 2, Laboratoire Charles Coulomb UMR 5221, F-34905 Montpellier, France*
[5]*CRHEA-CNRS, Rue Bernard Grégory, F-06560 Valbonne, France*

(Received 9 June 2014; accepted 24 June 2014; published online 7 July 2014)

We demonstrate a two-dimensional free-standing gallium nitride photonic crystal platform operating around 1550 nm and fabricated on a silicon substrate. Width-modulated waveguide cavities are integrated and exhibit loaded quality factors up to 34 000 at 1575 nm. We show the resonance tunability by varying the ratio of air hole radius to periodicity, and cavity hole displacement. We deduce a ~7.9 dB/cm linear absorption loss for the suspended nitride structure from the power dependence of the cavity in-plane transmission. © *2014 AIP Publishing LLC*.
[http://dx.doi.org/10.1063/1.4887065]

The nitride semiconductor materials are considered as the most appropriate materials for short wavelength and ultra-violet nanophotonics.[1–3] More recently, there has been an increased interest for using nitrides like gallium nitride or aluminum nitride in the near-infrared at telecom wavelengths. As opposed to silicon which is centrosymmetric, the nitride semiconductors exhibit a non-vanishing second-order nonlinear susceptibility[4] which can be used for second-order nonlinear processes (harmonic generation, frequency conversion). The mechanical properties and piezoelectricity of the nitrides could also be exploited for optomechanics.[5] As compared to III–V materials like InP or GaAs or silicon materials, the third order susceptibility for two-photon absorption is strongly decreased since two-photon absorption at 1.55 μm falls in the transparency window of gallium nitride.[6] The large band gap of the nitride is thus a very important asset. Furthermore, the nitrides exhibit a high thermal conductivity and could possibly support much higher pump power densities as compared to silicon. These properties are all the more interesting that the nitride can be integrated on silicon, thus offering a new platform for silicon photonics, using nitride as passive or active materials.[7,8] Integrating photonic crystals onto this platform brings higher functionalities for light propagation management and the realization of complex routing architectures with couplers, delay lines, etc. The index contrast between nitride (~2.3 at telecommunication wavelength) and air is important, thus allowing to fabricate cavities with high Q factors and small modal volumes.[9]

One of the interests associated with near-infrared nitride photonics platform is the possibility to develop two-dimensional planar photonic circuits where light can be coupled from the cleaved facets. This type of two-dimensional platform offers higher flexibility for characterization and future integration on chip. A first demonstration of such gallium nitride platform on silicon has been reported recently.[10] The investigated structures were composed of suspended ridge-access waveguides and two-dimensional photonic crystals. Quality factors up to 5400 for double heterostructure cavities at 1611 nm with in-line coupling were demonstrated with this platform.[11] It is worth noting that very high quality factors up to 148 000 at 1530 nm were also obtained with suspended aluminum nitride nanobeam cavities fabricated with sputter-deposited AlN-on-insulator substrates.[12] In the latter case, input and output light were distributed with grating couplers. One of the drawback is that the tuning of the nanobeam cavity resonance is less practical as compared to a two-dimensional photonic crystal where heating elements and metal pads can be deposited in close proximity with the photonic crystal cavities.[13]

In this work, we demonstrate a gallium nitride two-dimensional photonic crystal platform operating around 1550 nm. The platform consists of free-standing ridge nitride waveguides suspended by nanotethers and suspended two-dimensional photonic crystal nitride membranes grown on a silicon substrate. We report loaded quality factors for width-modulated waveguide cavities up to 34 000. We illustrate the tuning capacity of this system by varying the photonic crystal parameters. We have finally investigated the cavity response as a function of the incident power. We deduce the value of the residual linear absorption in suspended gallium nitride from the red-shift of the resonance at high pump powers.

The studied samples were grown by molecular beam epitaxy on a Si (111) substrate. The nitride layer consists of a thin AlN layer, around 45 nm thick, epitaxially grown on silicon followed by a 300 nm thick GaN layer. Two samples with total thicknesses of 330 and 345 nm were studied. There is some residual stress in the GaN layer as well as a strain gradient along the vertical direction. This strain gradient results from the compressive strain relaxation when growing GaN on AlN. The relaxation profile in GaN depends on the

a)Electronic mail: philippe.boucaud@ief.u-psud.fr. URL: http://pages.ief.u-psud.fr/QDgroup

structural quality of the thin AlN buffer layer. The residual stress results from this compressive strain gradient and the tensile strain induced by the difference of thermal dilatation coefficients between nitrides and the silicon substrate when going from epitaxy temperature to room temperature. The structural quality of the thin AlN layer has an impact on the residual stress and on the structural quality of the GaN layer. For processing, an oxide layer was first deposited on the sample. The electronic lithography of the waveguides and photonic crystal patterns was then performed in a single step. The pattern was transferred by reactive ion etching into the oxide layer. We then did etch the nitride material using chlorine-based inductively coupled plasma (ICP) etching with a mixture of Cl_2, BCl_3, and Ar gases (25/10/5 SCCM). The ICP etching rate is 400 nm/min. The selectivity with the oxide mask is 1:16. The oxide mask was removed after ICP etching using a buffered fluorhydric acid solution and before the release of the membrane. Dies with a total length of 500 μm were obtained by saw dicing. The silicon was then selectively etched using XeF_2 to release the suspended structures, with an etching depth between 1.5 and 5 μm. The two-dimensional photonic crystal has a length between 18 and 24 μm. Light is guided by a W0.98 waveguide corresponding to a width of $0.98\sqrt{3}a$, where a is the photonic crystal lattice periodicity (580 nm). The hole radius to periodicity ratio was varied around 0.23. We have designed width-modulated waveguide cavities following the A1 design presented in Ref. 14 (see inset of Fig. 3(b)). The design of these cavities consists in shifting laterally 30 holes around the cavity center with a maximum hole displacement of 15 nm. The cavity is coupled to the access ridge waveguides by barrier coupling waveguides with a length that can be varied between 13 and 17 lattice periodicities. These in-line coupling waveguides control the cavity transmission and have an impact on the loaded quality factor. Light is injected in the photonic crystal from the diced sample edge through ridge waveguides suspended by nanotethers following the design presented in Ref. 15. The tethers have a 140 nm width at the waveguide side and 350 nm width at the blanket side. The number of supporting tethers was varied between 16 and 36 for the whole suspended structure corresponding to a spacing of 12 and 27 μm. We used a non-periodical tether positioning in order to avoid Bragg resonances with large amplitudes in the transmission spectra. For transmission measurements, light is injected with lensed fibers through tapers in order to optimize the coupling efficiency. The taper length is 12 μm. Figure 1(a) shows an optical microscopy image of the whole structure. Figure 1(b) shows a scanning electron microscopy image of the transition between the ridge waveguide and the photonic crystal and Figure 1(c) shows a zoom around the access taper. The coupling efficiency was first characterized by using suspended waveguides without photonic crystals. Fig. 1(d) shows the transmission losses as a function of the number of tethers. The transmission in dB depends linearly on the number of tethers. The extrapolation of the curve to zero tether indicates that the coupling losses are 10 dB, if we neglect the linear absorption losses, as justified below. If we subtract the 3 dB losses measured without sample, we obtain a total 7 dB loss corresponding to coupling losses of 3.5 dB for each taper. These values could obviously be optimized

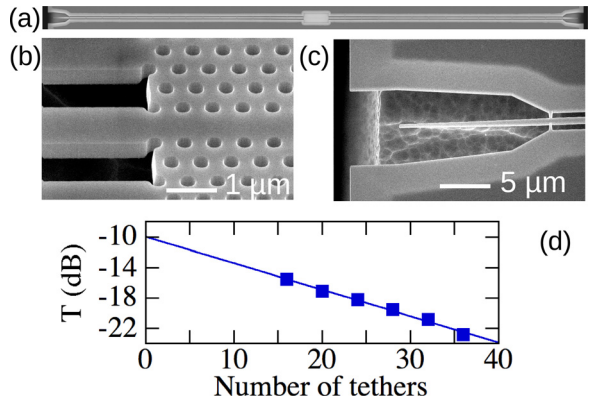

FIG. 1. (a) Optical, microscopy image of the two-dimensional photonic crystal platform with the photonic crystal at the center, and the access waveguides suspended by nanotethers. The total structure length is 500 μm. (b) Zoom at the transition between the ridge waveguide and the photonic crystal. (c) Zoom around the coupling taper for light injection/collection with lensed fibers. (d) Transmission losses for 500 μm long structures without photonic crystals as a function of the number of tethers. The full line is a linear fit. Its extrapolation to zero gives the coupling losses due to both tapers and experimental setup.

by design and fabrication but we are already very close to the performances obtained with similar structures on silicon. For the structure with 16 tethers, the scattering losses are 5.5 dB for a 500 μm length, corresponding to a 11 dB/mm propagation loss for this gallium nitride suspended structure. This value is equivalent than the one reported in Ref. 10 (12 dB/mm).

Figure 2 shows a transmission spectrum measured for a structure with a 24 μm photonic crystal and supported by 14 nanotethers on each side of the photonic crystal. A width-modulated waveguide cavity with a maximum hole displacement of 12 nm is located at the center of the photonic crystal.

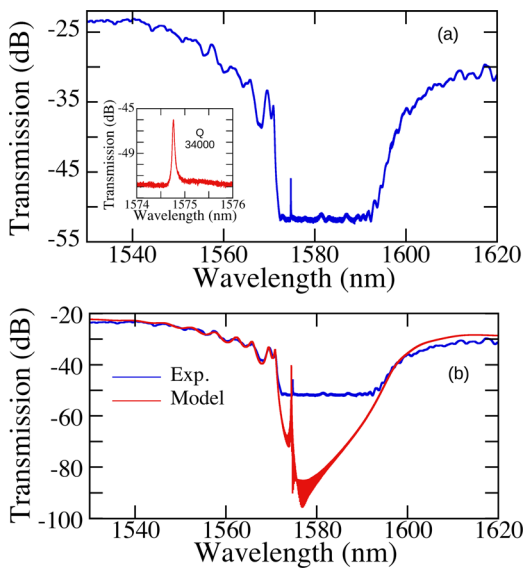

FIG. 2. (a) Transmission of a structure constituted of a 24 μm long photonic crystal with a width-modulated waveguide cavity. The number of supporting tethers on each side of the photonic crystal is 14. The maximum displacement of the cavity hole is 12 nm. The barrier coupling length between cavity and ridge waveguide is 17 *a*. The inset shows a zoom around the resonance of the cavity fundamental mode. A loaded quality factor of 34 000 is measured. (b) Comparison between the experimental transmission spectrum and the calculated one (red curve) using Meep software. The Q factor of the resonance is limited by the modeling time.

The lattice periodicity a is 580 nm and the air hole radius ratio to periodicity $\frac{r}{a}$ is 0.23. The length of the coupling waveguides between the photonic crystal edge and the cavity is $17\,a$. The thickness of the AlN+GaN layer is 345 nm. In order to obtain the full dynamical range, the spectrum is measured with two sensitivities on the oscilloscope. Outside the photonic crystal band gap, the transmission losses are −23 dB at 1520 nm, including 19.5 dB losses associated with tapers and tethers. The photonic band gap of the W0.98 waveguide is clearly observed between 1570 and 1590 nm. The oscillations observed around the base line at −52 dB are attributed to a residue due to a TM-polarized mode. The visibility of this residue depends on the silicon etching depth and on the taper size. Two factors can explain the conversion of TE-polarized light to TM polarized light. The vertical stack is intrinsically asymmetric as aluminum nitride and gallium nitride have different refractive indices. The etching of the holes is not perfectly vertical, with a 4° residual inclination, thus leading to TE-to-TM conversion.[8] The striking feature reported in Fig. 2 is the presence of a resonant mode around 1575 nm which is attributed to the fundamental mode of the width-modulated waveguide cavity. The inset of Fig. 2 shows a zoom around this resonance, with a measured loaded quality factor of 34 000, much larger than those previously reported in similar architectures.[11] The loaded quality factor Q_l results from the cavity quality factor Q_{cav} and the coupling quality factor Q_c following $\frac{1}{Q_l} = \frac{1}{Q_{cav}} + \frac{1}{Q_c}$. The cavity transmission at resonance is equal to $\left(\frac{Q_l}{Q_c}\right)^2$. Considering a −26.5 dB transmission at resonance between the access waveguides before and after the photonic crystal, it gives a coupling quality factor of 718 500 and a cavity quality factor of 35 690. This value still remains significantly smaller than the theoretical intrinsic value (490 000). This origin of the difference is discussed below. Fig. 2(b) shows a comparison between the transmission spectrum and the theoretical one as obtained by finite difference in time domain modeling using the Meep software.[16] A good agreement is obtained, in particular, for the band gap spectral width and the resonant position of the fundamental mode of the width-modulated waveguide cavity. The modeling does not account for the residual TM-mode.

Figure 3 shows examples of the large tunability that can be achieved with this system and the capability to tune the resonance wavelength into the C-band (1530–1565 nm). The measurements were performed with the 330 nm thick sample and the residual TM mode is hardly visible in these measurements. Fig. 3(a) shows the transmission dependence as a function of the $\frac{r}{a}$ ratio. The photonic crystal band gap increases significantly as $\frac{r}{a}$ increases. As expected, the cavity transmission also decreases as $\frac{r}{a}$ increases while the length of the photonic crystal barrier waveguide is kept constant. Fig. 3(b) depicts the transmission dependence as a function of the hole displacement of the width-modulated waveguide cavity. The increase of displacement leads to a red-shift of the resonance cavity, along with an increase of the quality factor. We have also checked the dependence of the cavity transmission amplitude as a function of the length of the coupling barrier waveguide (not shown). Decreasing this parameter leads to an increase of the transmission at the expense of the loaded quality factor.

Two-photon absorption is a strongly limiting factor of Si, InP, or GaAs for photonic circuit applications around 1.55 μm, as it leads to saturation of transmission in resonant cavities as pump power is increased. This saturation results from resonance shift due to a combination of free carrier absorption-dispersion and thermal effect. Due to its much larger band gap, it is expected that residual two-photon absorption is much weaker in GaN. We have thus investigated the pump power dependence of a cavity similar to the one presented in Fig. 2 (Q_l factor around 31 000, number of tethers 16). Figure 4 shows the measurements at different

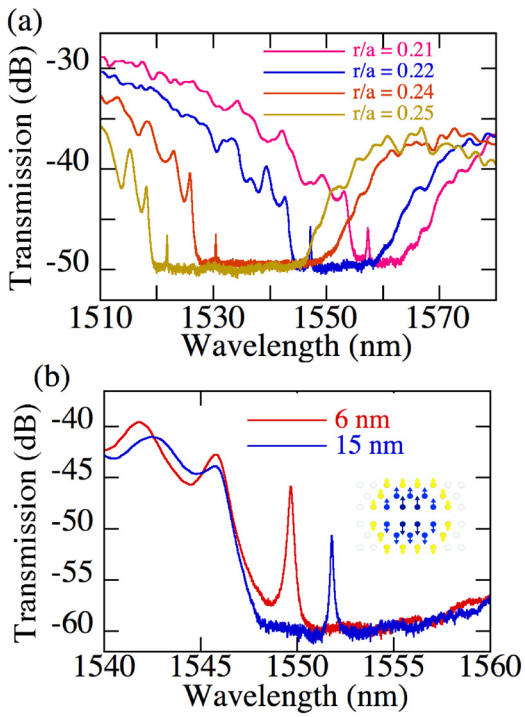

FIG. 3. (a) Transmission dependence as a function of $\frac{r}{a}$ ratio. The maximum hole displacement for the cavity is 9 nm. The barrier coupling length is 13 a. The sample thickness is 330 nm. (b) Transmission dependence as a function of lateral displacement for the width-modulated waveguide cavity. The inset shows a schematics of the lateral hole displacements for the cavity. The blue and yellow arrows correspond to 2/3 and 1/3 of the main displacement.

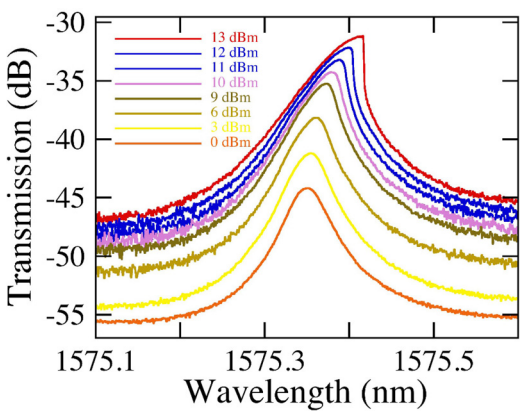

FIG. 4. Transmission of the resonance associated with a width-modulated waveguide cavity as a function of the pump power measured at the laser output. The Q_l factor at low excitation is 31 000. The number of supporting tethers is 16.

incident pump powers measured at the laser output. The resonance is red-shifted as the pump power is increased. We attribute this red-shift to a thermal effect due to residual linear absorption and we neglect the dispersion associated with free carrier generation. As the power continues to increase, the asymmetry of the resonance becomes more pronounced as a consequence of the wavelength sweep from short to long wavelength.[17] The output power follows a linear dependence as a function of the input power, indicating that the losses stem from linear absorption. One can estimate the absorbed power P_{abs} due to residual linear absorption from the spectral shift of the resonance following $\delta\lambda = \frac{\partial n}{\partial T} R_{th} P_{abs} \frac{\lambda}{n}$ and $P_{abs} = \frac{2\alpha c \gamma Q_l \sqrt{Tr_{max}}}{n \omega_0} P_{in} = 2\gamma \frac{Q_l^2}{Q_c Q_{abs}} P_{in}$, where $Q_{abs} = \frac{2\pi n}{\alpha\lambda}$ and γ is the fraction of the mode energy in the material (86%), n is the refractive index, $\frac{\partial n}{\partial T}$ is the thermo-optic coefficient, R_{th} is the thermal resistance. P_{in} is the input power at the entrance of the photonic crystal. α is the unknown linear absorption, Tr_{max} is the cavity transmission at resonance and low power. The contribution of thermal dilation to the wavelength shift is negligible. By considering a thermo-optic coefficient $\frac{\partial n}{\partial T}$ for GaN (Ref. 18) of 10^{-4} K^{-1} and a thermal resistance R_{th} of 5780 (K/W),[19] one deduces a linear absorption α of $1.8 \pm 0.4\,cm^{-1}$, i.e., 7.9 dB/cm at 1575 nm. We can note that a 7.9 dB/cm propagation loss gives an absorption quality factor Q_{abs} of about 49 800. The measured quality factor is thus mainly dominated by the linear absorption loss. The cavity quality factor Q_{cav} is equal to 32 200 $\left(\frac{1}{Q_l} = \frac{1}{Q_{cav}} + \frac{1}{Q_c};\ Q_c = 824\,824\right)$ and the intrinsic quality factor Q_{int} as given by $\frac{1}{Q_{cav}} = \frac{1}{Q_{int}} + \frac{1}{Q_{abs}}$ is equal to 91 000. We can also observe that the value of linear absorption indicates that the losses as discussed in Fig. 1(d) are dominated by the scattering losses due to the suspended nanotethers, thus making the measurement of the absorption losses challenging. The sensitivity of the photonic crystal resonance allows one to estimate this low absorption value.

In conclusion, we have demonstrated a free standing two-dimensional gallium nitride photonic crystal platform operating at the telecommunication wavelength. We have fabricated width-modulated waveguide cavities with quality factors up to 34 000, significantly larger than those previously published. We have investigated the pump power dependence of the cavity transmission. We have deduced a linear absorption of 7.9 dB/cm for the free-standing nitride, an absorption difficult to estimate in standard propagation measurements due to the predominance of scattering by nanotethers. This two-dimensional platform appears as very promising for nonlinear experiments with nitride semiconductors.

This work was supported by Agence Nationale de la Recherche under QUANONIC convention (ANR 2013BS10-0010-03). This work was also partly supported by the RENATECH network. We acknowledge support from GANEX (Grant No. ANR-11-LABX-0014). GANEX belongs to the public funded "Investissements d'Avenir" program managed by the French National Research Agency.

[1]D. Sam-Giao, D. Néel, S. Sergent, B. Gayral, M. J. Rashid, F. Semond, J. Y. Duboz, M. Mexis, T. Guillet, C. Brimont, S. David, X. Checoury, and P. Boucaud, Appl. Phys. Lett. **100**, 191104 (2012).
[2]S. Sergent, M. Arita, S. Kako, K. Tanabe, S. Iwamoto, and Y. Arakawa, Appl. Phys. Lett. **101**, 101106 (2012).
[3]M. Stegmaier, J. Ebert, J. M. Meckbach, K. Ilin, M. Siegel, and W. H. P. Pernice, Appl. Phys. Lett. **104**, 091108 (2014).
[4]Y. Fujii, S. Yoshida, S. Misawa, S. Maekawa, and T. Sakudo, Appl. Phys. Lett. **31**, 815–816 (1977).
[5]C. Xiong, W. H. P. Pernice, X. Sun, C. Schuck, K. Y. Fong, and H. X. Tang, New J. Phys. **14**, 095014 (2012).
[6]C.-K. Sun, J.-C. Liang, J.-C. Wang, F.-J. Kao, S. Keller, M. P. Mack, U. Mishra, and S. P. DenBaars, Appl. Phys. Lett. **76**, 439–441 (2000).
[7]C. Xiong, W. H. P. Pernice, and H. X. Tang, Nano Lett. **12**, 3562–3568 (2012).
[8]D. Néel, I. Roland, X. Checoury, M. El Kurdi, S. Sauvage, C. Brimont, T. Guillet, B. Gayral, F. Semond, and P. Boucaud, Adv. Nat. Sci.: Nanosci. Nanotechnol. **5**, 023001 (2014).
[9]X. Checoury, D. Néel, P. Boucaud, C. Gesset, H. Girard, S. Saada, and P. Bergonzo, Appl. Phys. Lett. **101**, 171115 (2012).
[10]U. Dharanipathy, N. Vico Trivino, C. Yan, Z. Diao, J.-F. Carlin, N. Grandjean, and R. Houdre, Opt. Lett. **37**, 4588–4590 (2012).
[11]N. Vico Trivino, U. Dharanipathy, J.-F. Carlin, Z. Diao, R. Houdre, and N. Grandjean, Appl. Phys. Lett. **102**, 081120 (2013).
[12]W. H. P. Pernice, C. Xiong, C. Schuck, and H. X. Tang, Appl. Phys. Lett. **100**, 091105 (2012).
[13]L.-D. Haret, X. Checoury, F. Bayle, N. Cazier, P. Boucaud, S. Combrié, and A. de Rossi, Opt. Express **21**, 10324–10334 (2013).
[14]E. Kuramochi, M. Notomi, S. Mitsugi, A. Shinya, T. Tanabe, and T. Watanabe, Appl. Phys. Lett. **88**, 041112 (2006).
[15]Z. Han, X. Checoury, D. Néel, S. David, M. El Kurdi, and P. Boucaud, Opt. Commun. **283**, 4387–4391 (2010).
[16]A. F. Oskooi, D. Roundy, M. Ibanescu, P. Bermel, J. Joannopoulos, and S. G. Johnson, Comput. Phys. Commun. **181**, 687–702 (2010).
[17]T. Uesugi, B. S. Song, T. Asano, and S. Noda, Opt. Express **14**, 377–386 (2006).
[18]N. Watanabe, T. Kimoto, and J. Suda, J. Appl. Phys. **104**, 106101 (2008).
[19]L.-D. Haret, A. Ghrib, X. Checoury, N. Cazier, Z. Han, M. El Kurdi, S. Sauvage, and P. Boucaud, Opt. Lett. **39**, 458–461 (2014).